Optical absorption of Er^{3+} in $RbTiOPO_4$ and $KTiOPO_4$

1998 J. Phys.: Condens. Matter 10 10101

(http://iopscience.iop.org/0953-8984/10/44/015)

J. Phys.: Condens. Matter **10** (1998) 10101–10113. Printed in the UK PII: S0953-8984(98)95593-X

Optical absorption of Er^{3+} in $RbTiOPO_4$ and $KTiOPO_4$

M Rico†, C Zaldo†§, J Massons‡ and F Díaz‡

† Instituto de Ciencia de Materiales de Madrid, Consejo Superior de Investigaciones Científicas, Cantoblanco, 28049 Madrid, Spain

‡ Laboratori de Física Aplicada i Cristal.lografia, Universitat Rovira i Virgili, 43005 Tarragona, Spain

Received 6 July 1998

Abstract. The optical absorption of Er^{3+} in $RbTiOPO_4$ (RTP) and $KTiOPO_4$ (KTP) single crystals has been characterized at 5 K and 300 K temperatures. The room temperature oscillator strengths of Er^{3+} obtained in both lattices are similar although in KTP the uncertainty is higher due to the lower concentration of Er in the samples available. The results obtained in RTP have been analysed by using the Judd–Ofelt theory. The effective Judd–Ofelt parameters obtained for Er^{3+} in RTP are $\Omega_2^{eff} = 12.85 \times 10^{-20}$ cm^2, $\Omega_4^{eff} = 0.60 \times 10^{-20}$ cm^2, $\Omega_6^{eff} = 0.57 \times 10^{-20}$ cm^2. The photoluminescence transition radiative rates, branching ratios and radiative lifetimes of Er^{3+} in these crystals have been calculated for all de-excitations from the $^4G_{9/2}$ multiplet. The $^4I_{13/2} \rightarrow {}^4 I_{15/2}$ erbium emission has been characterized. The low temperature optical absorption and photoluminescence suggest the coexistence of two erbium centres in both lattices, which we have tentatively ascribed to the occupancy with different population densities of the two titanium lattice sites.

1. Introduction

The isomorphous $RbTiOPO_4$ (RTP) and $KTiOPO_4$ (KTP) single crystals are important non-linear optical (NLO) materials for frequency doubling the 1.06 μm neodymium laser emission. This has been shown in bulk crystals [1], waveguides [2] and in quasiphase-matched periodically poled waveguides [3, 4]. These crystals have also found applications as optical parametric devices [5]. As a consequence of the great difficulty in incorporating rare earths (RE) into the crystal lattice, the spectroscopic properties of rare earths in these materials have been considered only recently [6–8].

To grow these crystals a flux is required, since KTP melts incongruently in air at 1172 °C [9] and its surface decomposes at even lower temperatures $\geqslant$900 °C [10]. It has been shown recently that the low RE concentration in these crystals is due to the modification of the phases which first nucleate in the flux [11]. Above a certain RE concentration in the flux the region where RTP or KTP nucleate disappears. Moreover, the distribution coefficients for the incorporation of RE from the flux to the crystal are low, typically in the 0.5–6 $\times 10^{-3}$ range. The final Er concentration obtained in the crystal is about 10^{18} cm^{-3}. In order to obtain higher erbium concentrations, ion beam mixing [12] and thermal diffusion [13] have been used to incorporate Er into the sample surface reaching erbium concentrations of about 10^{20}–10^{21} cm^{-3}. To explore the optical applications of these devices, the spectroscopic properties of Er in these hosts must be known.

§ Corresponding author. E-mail address: cezaldo@icmm.csic.es.

0953-8984/98/4410101+13$19.50

A priori, the possible lattice sites that can be envisaged for rare-earth ions in RTP or KTP crystals are the Ti sites and the Rb (or K) sites. Phosphorus sites can be excluded in view of the small ionic radius of P^{5+} (0.34 Å) and its tetrahedral coordination in the lattice. The ionic radius of Ti^{4+} is 0.68 Å, being octahedrally coordinated with oxygens; while the large K^+, with ionic radius of 1.33 Å, is weakly bonded to the lattice with a high coordination number. The fact that the distribution coefficient of RE increases as the ionic radius of the impurity decreases suggests that rare-earth ions mainly replace titanium. Even in that case, at least two different centres may be expected, since the crystal structure has two inequivalent positions for each cation [14].

In previous works [6, 7] the optical absorptions of other RE ions, namely Nd^{3+}, Ho^{3+} and Tm^{3+}, have been reported only at low temperature. Er^{3+} having an ionic radius smaller than Nd^{3+} and Ho^{3+} is more efficiently incorporated into the lattice. This allows us to observe most of the optical absorption multiplets of the ion even at room temperature and therefore to use the theory developed by Judd and Ofelt [15, 16] to evaluate the expected photoluminescence properties of the ion in these lattices. The presence of several Er^{3+} centres and their local symmetry is studied by monitoring the optical absorption of Er^{3+} at 4 K, since the splitting of the erbium multiplets is a function of the site symmetry. Moreover, the Er^{3+} photoluminescence emission at about 1.5 μm, which is of interest in the optical communications systems [17] has been studied.

2. Experimental techniques

Er-doped RTP and KTP crystals have been grown by the top-seeded solution growth technique using K_2O–P_2O_5–TiO_2–Er_2O_3 flux. Details on the growth procedures have been given previously [11]. Prismatic samples used were orientated by standard x-ray diffraction techniques and cut with their faces perpendicular to the crystallographic axes $\boldsymbol{a}$, $\boldsymbol{b}$, $\boldsymbol{c}$. The $a\times b\times c$ dimensions of the samples used were $2\times2\times3$ mm^3 for the RTP and $3\times6.5\times6.5$ mm^3 for the KTP one.

The erbium concentration of the samples used have been obtained by Rutherford back-scattering technique. The erbium concentrations determined are $N_{Er,RTP} = 5 \times 10^{18}$ cm^{-3} and $N_{Er,KTP} = 1 \times 10^{18}$ cm^{-3}. The error of this determination is not larger than 20%; however due to the overlapping of the Er signal with that corresponding to Ti, the crystal depth analysed is lower than 600 nm. A twin KTP sample was dissolved and analysed by atomic absorption spectroscopy using PYE UNICAM SP-192 equipment. The Er concentration obtained was 3.3×10^{18} cm^{-3}. Further, in the KTP sample the intensity of the optical absorption was observed to depend slightly on the incident beam position, which shows that the erbium was not uniformly distributed; this contributes to a larger uncertainty of the oscillator strengths reported in table 1 for the KTP sample with regard to the RTP one. To average the uncertainty of the erbium concentration we have used in the next section an erbium concentration between the RBS and AA results and keeping the ratio obtained by RBS between the RTP and KTP samples, namely $\bar{N}_{Er,RTP} = 1 \times 10^{19}$ cm^{-3} and $\bar{N}_{Er,KTP} = 2 \times 10^{18}$ cm^{-3}.

Optical absorption measurements have been performed in a Varian 5E spectrophotometer. The temperature of the sample was varied in the range 5–300 K using an Oxford cryostat model SU12 and a Lake-Shore Cryotronics temperature controller, model DRC 91C. Polarized measurements were performed using a Glan–Thompson polarizer in the incident beam and a depolarizer plate in the transmitted beam.

Photoluminescence measurements have been excited with the 488 nm line of an Ar laser. The excitation beam was polarized along the *c*-axis of the samples. The emitted light

Table 1. Average wavelengths, $\bar{\lambda}$, experimental, $f_{ED,exp,}$ and calculated, $f_{ED,th,}$ electric dipolar oscillator strengths of Er^{3+} multiplets in RTP and KTP single crystals. The quality of the fit is described by the RMS(Δf) parameter.

		RTP						KTP		
		$10^6 \times f_{ED,exp}$			$10^6 \times f_{ED,th}$			$10^6 \times f_{ED,exp}$		
$^4I_{15/2} \rightarrow {}^{2S+I}L_J$ Transition	$\bar{\lambda}$ (nm)	$\parallel a$	$\parallel b$	$\parallel c$	$\parallel a$	$\parallel b$	$\parallel c$	$\parallel a$	$\parallel b$	$\parallel c$
$^4G_{9/2}$	366	1.52	2.45	3.79	0.53	0.68	1.12	2	3	5
$^4G_{11/2}$	378.5	29.97	39.83	63.10	28.65	40.20	56.03	25	31	47
$^2H_{9/2}$	408				0.50	0.28	0.53			
$^4F_{3/2}$	443				0.25	0.12	0.23			
$^4F_{5/2}$	452.5				0.43	0.21	0.40			
$^4F_{7/2}$	490	0.47	0.19	0.47	1.19	0.75	1.36			
$^2H_{11/2}$	521	14.15	21.56	22.90	15.33	21.24	28.96	5	14	17
$^4S_{3/2}$	544	2.02	1.72	2.67	0.34	0.16	0.32	2	3	4
$^4F_{9/2}$	652	0.77	0.58	1.06	0.85	0.88	1.44			
$^4I_{9/2}$	810				0.08	0.16	0.24			
$^4I_{11/2}$	980				0.63	0.58	0.86			
$^4I_{13/2}$	1536				0.90	0.55	0.94			
$10^6 \times$ RMS(Δf)					1.37	1.24	5.00			

was analysed with a Spex 340E (focal length, 34 cm) monochromator and detected with a Ge photodiode, model ADC-403IR, cooled at 77 K. The signal of the photodiode was recorded by using a lock-in amplifier.

3. Experimental results and discussion

3.1. Room temperature optical absorption

The optical absorption of Er^{3+} in single crystals is characterized by $^{2S+1}L_J$ multiplets which degeneracy is partially lifted by the crystal field giving rise to Stark sublevels. In RTP and KTP, the multiplets lying at an energy higher than 20 000 cm^{-1} are overlapped with a background absorption due to point defects of the lattice [18]. In order to minimize this absorption, before the measurements the samples were heated for 2 h to 200 °C, moreover the residual background absorption was analytically evaluated in the side regions of each multiplet and discounted of the spectra measured.

Figure 1 shows the room temperature (RT) unpolarized optical absorption spectra of Er^{3+} in RTP and KTP crystals. The band sets observed have been labelled according to the energy level diagram reported for erbium, whose average positions are little sensitive to the host [19]. Due to the higher Er concentration of the RTP sample the spectrum is better defined. In this sample eight multiplets can be clearly resolved, namely $^4G_{9/2}$, $^4G_{11/2}$, $^2H_{9/2}$, $^4F_{7/2}$, $^2H_{11/2}$, $^4S_{3/2}$, $^4F_{9/2}$ and $^4I_{13/2}$. In KTP the number of multiplets showing significant intensity is smaller; only the $^4G_{9/2}$, $^4G_{11/2}$, $^2H_{11/2}$ and $^4S_{3/2}$ can be reliably resolved from the noise.

Further, polarized optical absorption spectra have been recorded parallel to the three crystallographic axes. The results are not shown for the sake of brevity but the main conclusions are similar to those shown later at 5 K, namely the most intense absorption is generally found for light polarized parallel to the crystallographic *c*-axis and the weakest one for light polarized parallel to the *a*-axis.

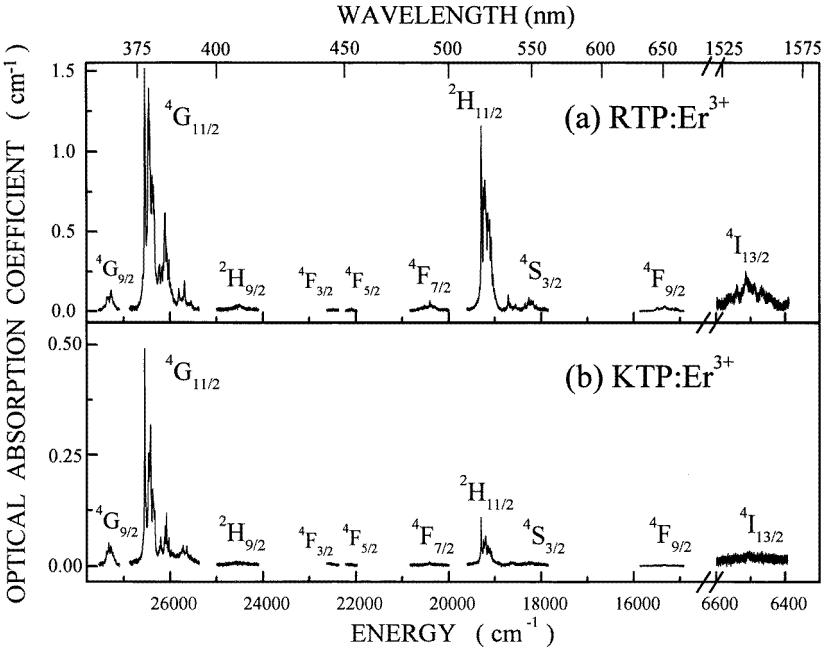

Figure 1. Unpolarized optical absorption spectra of Er^{3+} in RTP (a) and KTP (b) obtained at 300 K.

The experimental oscillator strengths, f_{exp}, of the $J \rightarrow J'$ transition (J being the $^4I_{15/2}$ fundamental multiplet) are obtained from the experimental spectra by

$$f_{exp} = \frac{2mc}{\alpha_f h N \bar{\lambda}^2} \int_{JJ'} \alpha(\lambda)\, \mathrm{d}\lambda \tag{1}$$

where m is the electron mass, c the vacuum speed of light, α_f the fine-structure constant, h the Planck constant, N the erbium concentration, $\bar{\lambda}$ the average wavelength and $\int_{JJ'} \alpha(\lambda)\, \mathrm{d}\lambda$ the integrated absorption of the $J \rightarrow J'$ transition.

With the exception of the $^4I_{15/2} \rightarrow {}^4I_{13/2}$ transition, the optical absorption of Er^{3+} corresponds to electric dipolar transitions. Even though this transition has been observed in RTP, it has not been used in the Judd–Ofelt (JO) treatment because of the high uncertainty in the baseline correction. Table 1 summarizes the average wavelength considered for each multiplet and the experimental oscillator strengths obtained. The experimental oscillator strengths of Er^{3+} in RTP and KTP lattices are in the same order of magnitude; however the error in the determination of those corresponding to Er^{3+} in KTP is larger because of the larger uncertainty in the baseline correction and the more inhomogeneous distribution of the impurity in the KTP sample. The oscillator strength error estimated for the values reported in table 1 is about 0.01×10^{-6} and 0.5×10^{-6} for RTP and KTP respectively.

For electric dipole transitions, the JO theory gives the theoretical oscillator strengths as a function of the Ω_k ($k = 2, 4, 6$) JO parameters as

$$f_{ED,th} = \chi \left[\frac{8\pi^2 mc}{h}\right] \frac{1}{3\bar{\lambda}(2J+1)} \sum_{k=2,4,6} \Omega_k |\langle 4f^N \alpha[SL]J \| U^\lambda \| 4f^N \alpha'[S'L']J' \rangle|^2 \tag{2}$$

where $\chi = (n^2+2)^2/9n$. The refractive indices of RTP were obtained from the work of

Cheng *et al* [20] and the reduced matrix elements corresponding to the $J \rightarrow J'$ transition of Er^{3+}, $|\langle\|U^{\lambda}\|\rangle|^2$, were obtained by Weber [21] and Carnall [22].

The minimization of the difference between the experimental and theoretical oscillator strengths given by $\sum_{J'}(f_{exp} - f_{ED,th})^2$, yields the Ω_k set corresponding to Er^{3+} in the considered host. The quality of the fit is characterized by the root-mean-square (RMS) deviation parameter defined as

$$\mathrm{RMS}(\Delta f) = \left(\left(\sum_{i=1}^{i=l}(f_{ED,exp} - f_{ED,th})^2\right)(\text{No transitions} - \text{No parameters})^{-1}\right)^{1/2}. \tag{3}$$

Table 2 gives the Judd–Ofelt parameters obtained for Er^{3+} in the RTP lattice. We have calculated the $\Omega_k^{a(b\ or\ c)}$ sets using the refractive index corresponding to each axis and the effective Ω_k^{eff} parameters were calculated as $\Omega_k^{eff} = 1/3(\Omega_k^a + \Omega_k^b + \Omega_k^c)$. In KTP such a treatment has not been intended in view of the large uncertainty of the experimental oscillator strengths.

Table 2. Judd–Ofelt parameters of Er^{3+} in $RbTiOPO_4$ single crystal. Ω_k^i $(i = a, b, c)$ have been obtained from the polarized absorption. $\Omega_k^{eff} = 1/3\Sigma_i\ \Omega_k^i$ is the effective JO parameter.

	Ω_k^a	Ω_k^b	Ω_k^c	Ω_k^{eff}
$10^{20} \times \Omega_2$ (cm^2)	9.46	12.91	16.20	12.85
$10^{20} \times \Omega_4$ (cm^2)	0.28	0.64	0.89	0.60
$10^{20} \times \Omega_6$ (cm^2)	0.74	0.35	0.63	0.57

The Ω_2^{eff} parameter obtained is in the upper limit of the values found in other oxides. However, it must be noticed that Ω_2 for Er^{3+} in phosphates always reaches rather high values [23], typically about 10×10^{-20} cm^2.

Once the Ω_k set is known, the electric dipole radiative emission rate of the $J \rightarrow J'$ transition, J being the excited state and J' the final state of the radiative transition, can be calculated as

$$A_{ED,JJ'} = \chi\left[\frac{32\pi^3 c\alpha_f}{3\bar{\lambda}^3}\right]\frac{n^2}{(2J+1)}\sum_{k=2,4,6}\Omega_k|\langle 4f^N\alpha[SL]J\|U^{\lambda}\|4f^N\alpha'[S'L']J'\rangle|^2. \tag{4}$$

The electric dipole approximation describes most of the photoluminescence properties of erbium. However magnetic dipolar transitions, with selection rules $\Delta S = \Delta L = 0$, $\Delta J = 0, \pm 1$, also contribute efficiently to some of the emission rates; in particular the $^4I_{11/2} \rightarrow {}^4I_{13/2}$ and $^4I_{13/2} \rightarrow {}^4I_{15/2}$ are affected significantly. This contribution is given by

$$A_{MD,JJ'} = \left[\frac{2\pi\alpha_f h^2}{3m^2 c}\right]\frac{n^3}{(2J+1)\bar{\lambda}^3}|\langle 4f^N\alpha[SL]J\|L + 2S\|4f^N\alpha'[S'L']J'\rangle|^2. \tag{5}$$

The expressions of the reduced matrix elements $|\langle\|L + 2S\|\rangle|^2$ have been reported by Carnall [24].

The total radiative rate $A_{JJ'}$ is obtained by addition of the electric and magnetic contributions. The transition branching ratios are given by

$$\beta_{JJ'} = A_{JJ'}\left(\sum_{J'}A_{JJ'}\right)^{-1} \tag{6}$$

and the radiative lifetimes are given by

$$\tau_{rJ} = \left(\sum_{J'} A_{JJ'} \right)^{-1}. \tag{7}$$

Table 3 summarizes the results obtained for all the multiplets with energy lower than the $^4G_{9/2}$ one assuming an average refractive index given by $\bar{n} = 1/3(n_a + n_b + n_c)$.

3.2. Low temperature optical absorption

The degeneracy of the $^{2S+1}L_J$ multiplets of rare earth ions is partially lifted by the interaction with the crystal field of the lattice. The number of sublevels arising with different energy depends on the crystal field symmetry, but for Er^{3+} the maximum number of sublevels expected for each multiplet is $(2J + 1)/2$ due to the Kramers degeneracy of its odd $4f^{11}$ electron configuration. Due to splitting of the $^4I_{15/2}$ ground multiplet of Er^{3+}, at 5 K only the fundamental sublevel is efficiently populated. This gives rise to narrow and intense optical absorption bands corresponding to transitions from the fundamental Stark sublevel of the $^4I_{15/2}$ multiplet to the sublevels of the excited multiplets.

Figure 2 shows the 5 K optical absorption of Er^{3+} in RTP recorded with light polarized parallel to the three crystallographic axes. The most intense spectrum is obtained for light polarized parallel to the *c*-axis, while the weakest one is observed when the light is polarized parallel to the *a*-axis. A similar conclusion is reached for Er^{3+} in KTP.

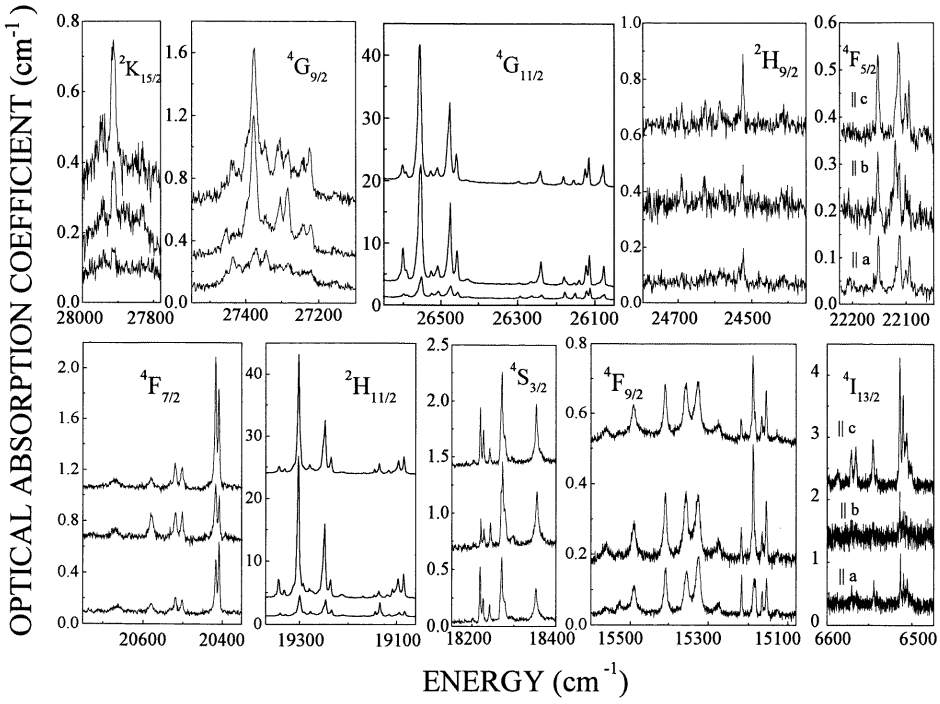

Figure 2. Polarized optical absorption spectrum of Er^{3+} in RTP obtained at 5 K.

It is worth noting that in many multiplets the number of peaks experimentally observed is larger than the maximum number of sublevels expected for a single erbium centre. To

Table 3. Emission wavelengths, electric dipolar and magnetic radiative transition rates, A, branching ratios, β, and radiative lifetimes, τ_{rad}, for Er^{3+} in RTP single crystals.

Transition	λ (nm)	$A_{ED} + A_{MD}$ (10^3 s^{-1})	β_{ij} (%)	τ_{rad} (μs)
$^4G_{9/2} \rightarrow$ $^4G_{11/2}$	5906	0.003	0	15
$^2H_{9/2}$	3 377	0.003	0	
$^4F_{3/2}$	2100	0.006	0.01	
$^4F_{5/2}$	1912	0.117	0.18	
$^4F_{7/2}$	1375	1.198	1.87	
$^2H_{11/2}$	1227	0.126	0.20	
$^4S_{3/2}$	1105	0.031	0.05	
$^4F_{9/2}$	817	2.322	3.62	
$^4I_{9/2}$	672	0.078	0.12	
$^4I_{11/2}$	587	2.663	4.15	
$^4I_{13/2}$	481	55.509	86.52	
$^4I_{15/2}$	367	2.103	3.28	
$^4G_{11/2} \rightarrow$ $^2H_{9/2}$	7886	0.001	0.00	12
$^4F_{3/2}$	3260	0.000	0.00	
$^4F_{5/2}$	2826	0.000	0.00	
$^4F_{7/2}$	1792	0.065	0.08	
$^2H_{11/2}$	1549	0.010	0.01	
$^4S_{3/2}$	1359	0.010	0.01	
$^4F_{9/2}$	948	2.128	2.53	
$^4I_{9/2}$	758	0.635	0.76	
$^4I_{11/2}$	652	0.048	0.06	
$^4I_{13/2}$	524	3.876	4.60	
$^4I_{15/2}$	391	77.466	91.95	
$^2H_{9/2} \rightarrow$ $^4F_{3/2}$	5555	0.000	0.00	239
$^4F_{5/2}$	4405	0.000	0.00	
$^4F_{7/2}$	2319	0.035	0.84	
$^2H_{11/2}$	1928	0.026 +0.012	0.91	
$^4S_{3/2}$	1642	0.000	0.00	
$^4F_{9/2}$	1077	0.043	1.03	
$^4I_{9/2}$	839	0.123	2.94	
$^4I_{11/2}$	711	0.665	15.90	
$^4I_{13/2}$	561	2.399	57.35	
$^4I_{15/2}$	412	0.880	21.03	
$^4F_{3/2} \rightarrow$ $^4F_{5/2}$	21 276	0.000	0.00	558
$^4F_{7/2}$	3981	0.000	0.00	
$^2H_{11/2}$	2951	0.000	0.00	
$^4S_{3/2}$	2331	0.025	1.40	
$^4F_{9/2}$	1337	0.015	0.85	
$^4I_{9/2}$	987	0.175	9.77	
$^4I_{11/2}$	815	0.607	33.85	
$^4I_{13/2}$	624	0.083	4.64	
$^4I_{15/2}$	445	0.887	49.49	
$^4F_{5/2} \rightarrow$ $^4F_{7/2}$	4897	0.005 +0.002	0.34	490
$^2H_{11/2}$	3427	0.002	0.10	
$^4S_{3/2}$	2618	0.003	0.15	
$^4F_{9/2}$	1427	0.076	3.73	
$^4I_{9/2}$	1035	0.136	6.68	
$^4I_{11/2}$	847	0.066	3.24	
$^4I_{13/2}$	643	0.772	37.90	
$^4I_{15/2}$	455	0.975	47.86	

Table 3. (Continued)

Transition	λ (nm)	$A_{ED} + A_{MD}$ (10^3 s^{-1})	β_{ij} (%)	τ_{rad} (μs)
$^4F_{7/2} \rightarrow {}^2H_{11/2}$	11 415	0.000	0.00	417
$^4S_{3/2}$	5624	0.000	0.00	
$^4F_{9/2}$	2013	0.010 +0.023	1.37	
$^4I_{9/2}$	1313	0.107	4.46	
$^4I_{11/2}$	1025	0.131	5.46	
$^4I_{13/2}$	740	0.252	10.51	
$^4I_{15/2}$	501	1.876	78.20	
$^2H_{11/2} \rightarrow {}^4S_{3/2}$	10 087	0.000	0.00	42
$^4F_{9/2}$	2444	0.103	0.43	
$^4I_{9/2}$	1484	0.265	1.12	
$^4I_{11/2}$	1126	0.126	0.53	
$^4I_{13/2}$	791	0.247	1.04	
$^4I_{15/2}$	524	23.056	96.88	
$^4S_{3/2} \rightarrow {}^4F_{9/2}$	3 136	0.000	0.03	858
$^4I_{9/2}$	1714	0.036	3.12	
$^4I_{11/2}$	1253	0.023	1.98	
$^4I_{13/2}$	852	0.312	26.83	
$^4I_{15/2}$	550	0.792	68.04	
$^4F_{9/2} \rightarrow {}^4I_{9/2}$	3778	0.010	1.04	1044
$^4I_{11/2}$	2088	0.068	7.08	
$^4I_{13/2}$	1170	0.068	7.09	
$^4I_{15/2}$	667	0.811	84.79	
$^4I_{9/2} \rightarrow {}^4I_{11/2}$	4668	0.000 +0.002	1.85	9142
$^4I_{13/2}$	1695	0.032	29.63	
$^4I_{15/2}$	810	0.074	68.52	
$^4I_{11/2} \rightarrow {}^4I_{13/2}$	2662	0.018 +0.016	14.47	4255
$^4I_{15/2}$	980	0.201	85.53	
$^4I_{13/2} \rightarrow {}^4I_{15/2}$	1536	0.086 +0.058	100	6944

illustrate this situation figure 3 shows the details of the optical absorption for the two most intense multiplets of erbium in RTP and KTP, namely $^4G_{11/2}$ and $^2H_{11/2}$. These spectra evidence the presence of more than one site for Er in RTP and KTP lattices. Table 4 gives the energy positions of the different absorption bands observed for each multiplet. In the RTP lattice the number of bands observed for the intense $^4G_{11/2}$ and $^2H_{11/2}$ multiplets agrees with the presence of two erbium centres. This is also observed in the $^4F_{7/2}$ and $^4F_{9/2}$ multiplets. In the other multiplets, whose intensity is low, the contribution of these two centres may be overlapped, contributing to the band-width, or the intensity of some bands may be comparable to the noise. Nevertheless, the presence of more than two centres cannot be excluded since in RTP the $^4S_{3/2}$ multiplet shows more than four bands. With only small changes, the positions of Er^{3+} bands are similar for the RTP and KTP lattices; however some relative changes in the intensities are observed.

The hypothesis of two sites for Er would agree with the occupancy of the two inequivalent titanium sites of the lattice, usually named as Ti1 and Ti2. These sites have C1 symmetry, therefore the expected number of bands observed for each sublevel would be $2(2J + 1)/2 \equiv 2J + 1$; this agrees with our experimental results in table 4.

Figure 4 shows the arrangement of the titanium sites in the lattice. As a first approximation we can imagine that the octahedra of oxygens around erbium were regular

Table 4. Position at 5 K of the Stark sublevels of Er^{3+} in RTP and KTP crystals. The $^4I_{15/2}$ multiplet has been characterized from the emission, the other multiplets from the optical absorption.

	E cm^{-1} (λ, nm)	
	$RbTiOPO_4$	$KTiOPO_4$
$^2K_{15/2}$	27 949 (357.80)	27 910 (358.30)
	27 914 (358.24)	27 878 (358.70)
$^2G_{9/2}$	27 375 (365.30)	27 386 (365.15)
	27 345 (365.70)	27 348 (365.66)
	27 303 (366.26)	27 300 (366.30)
	27 284 (366.52)	27 276 (366.62)
	27 223 (367.34)	27 223 (367.34)
	27 438 (364.46)	—
	27 456 (364.22)	27 456 (364.22)
	27 243 (367.07)	—
$^4G_{11/2}$	26 601 (375.92)	26 600 (375.94)
	26 556 (376.56)	26 589 (376.10)
	26 527 (376.98)	26 533 (376.90)
	26 510 (377.22)	26 506 (377.28)
	26 476 (377.70)	26 456 (377.78)
	26 459 (377.94)	26 456 (377.98)
	26 242 (381.08)	26 230 (381.24)
	26 181 (381.95)	26 175 (382.04)
	26 155 (382.34)	26 164 (382.20)
	26 125 (382.78)	26 123 (382.80)
	26 115 (382.92)	26 104 (383.08)
	26 079 (383.46)	26 076 (383.50)
$^2H_{9/2}$	24 690 (405.02)	—
	24 627 (406.06)	24 628 (406.05)
	24 588 (406.70)	24 597 (406.55)
	24 524 (407.76)	24 524 (407.76)
	24 414 (409.60)	24 416 (409.57)
$^4F_{3/2}$	22 572 (443.02)	22 558 (443.30)
	22 492 (444.60)	—
$^4F_{5/2}$	22 152 (451.42)	22 152 (451.43)
	22 120 (452.08)	22 119 (452.10)
	22 102 (452.44)	22 101 (452.47)
	22 112 (452.24)	—
	22 096 (452.58)	—
$^4F_{7/2}$	20 673 (483.72)	20 677 (483.63)
	20 581 (485.88)	20 580 (485.90)
	20 520 (487.32)	20 532 (487.04)
	20 418 (489.76)	20 432 (489.44)
	20 504 (487.72)	—
	20 409 (489.98)	—
$^2H_{11/2}$	19 342 (517.00)	19 347 (516.88)
	19 331 (517.30)	—
	19 301 (518.10)	19 303 (518.06)
	19 279 (518.70)	19 289 (518.44)
	19 249 (519.52)	19 249 (519.52)
	19 237 (519.84)	19 239 (519.78)
	19 145 (522.32)	19 143 (522.38)

Table 4. (Continued)

	E cm^{-1} (λ, nm)	
	$RbTiOPO_4$	$KTiOPO_4$
$^2H_{11/2}$	19 136 (522.57)	19 125 (522.88)
	19 116 (523.12)	19 119 (523.06)
	19 109 (523.32)	19 105 (523.42)
	19 097 (523.64)	19 092 (523.78)
	19 085 (523.96)	19 073 (524.31)
$^4S_{3/2}$	18 353 (544.89)	18 353 (544.86)
	18 297 (546.53)	18 294 (546.62)
	18 272 (547.30)	18 273 (547.25)
	18 228 (584.62)	18 226 (548.66)
	18 242 (548.18)	18 266 (547.48)
	18 220 (548.86)	18 221 (548.82)
$^4F_{9/2}$	15 562 (642.60)	15 558 (642.75)
	15 491 (645.55)	15 496 (645.34)
	15 409 (648.96)	15 403 (649.24)
	15 356 (651.20)	15 353 (651.34)
	15 324 (652.58)	15 339 (651.94)
	15 276 (654.62)	15 256 (655.49)
	15 219 (657.08)	15 218 (657.14)
	15 189 (658.38)	15 197 (658.04)
	15 166 (658.38)	15 187 (658.46)
	15 156 (659.82)	15 163 (659.52)
$^4I_{13/2}$	6588 (1518.00)	—
	6571 (1521.88)	—
	6566 (1523.10)	6567 (1522.87)
	6545 (1528.00)	6545 (1527.90)
	6514 (1535.14)	6511 (1535.80)
	6510 (1536.02)	6508 (1536.64)
	6506 (1536.96)	6504 (1537.50)
$^4I_{15/2}$		190
		169
		135
		106
		79
		67
		32
		0

and that the C_2 and C_4 symmetry axes of the octahedra were parallel to the crystallographic axes. In that case if both sites were equally populated, only slight intensity differences may be found between the absorption spectra recorded with light polarized parallel to the *a*-axis or *b*-axis. In these two latter configurations the spectra would be the superposition of a C_2 contribution of one site and the C_4 contribution of the other site. However, the light polarized parallel to the crystallographic *c*-axis is simultaneously parallel to the C_2 contributions of both sites and it would be expected to exhibit a spectrum different from the other two configurations. The experimental results shown in figure 2 do not support this model. The optical absorptions parallel to *a*-axis and *b*-axis are quite different, that recorded parallel to the *a*-axis being the weakest.

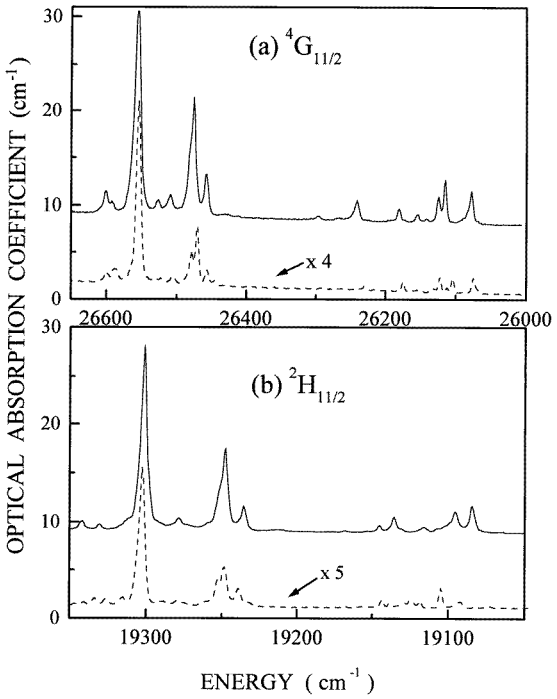

Figure 3. Comparison of the 5 K optical absorption spectra of Er^{3+} in RTP (solid line) and KTP (dashed line). (a) $^4I_{15/2} \rightarrow {}^4G_{11/2}$ transition, (b) $^4I_{15/2} \rightarrow {}^2H_{11/2}$ transition.

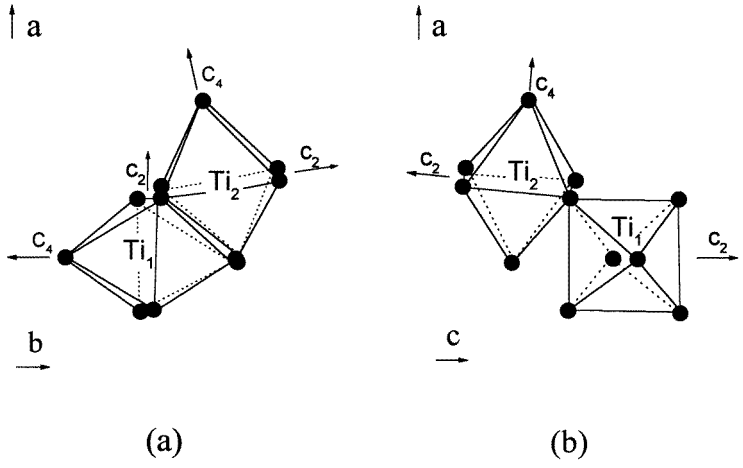

Figure 4. Schematic orientation of the oxygen octahedra around Ti ions in RTP and KTP lattices. (a) *c*-axis projection. (b) *b*-axis projection.

The results can be qualitatively understood assuming that the strongest absorption in both sites is parallel to the C_2 axis of the centre and that the Ti2 site is more populated than the Ti1. In this way, only the centre with lower population contributes to the absorption spectrum parallel to the *a*-axis, the centre with higher population mainly contributes to the

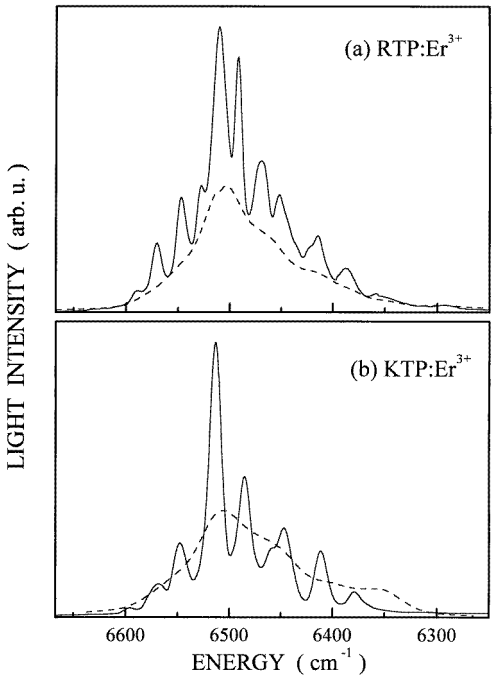

Figure 5. $^4I_{13/2} \rightarrow {}^4I_{15/2}$ emission of Er^{3+} in RTP (a) and KTP (b). The solid lines correspond to the spectra recorded at 5 K and the dashed lines to spectra recorded at 300 K.

absorption parallel to the *b*-axis and both centres contribute to the absorption parallel to the *c*-axis. The different erbium occupancy of the two titanium sites may be related to the different distortion of the oxygen quasi-octahedra of both lattice sites, that corresponding to Ti2 being the less distorted one.

3.3. Photoluminescence

Figure 5 shows the $^4I_{13/2} \rightarrow {}^4I_{15/2}$ photoluminescence emission of Er^{3+} observed after excitation of the $^4F_{7/2}$ level with the 488 nm light of a cw Ar laser.

At room temperature the spectra are broad and their structure cannot be resolved. In order to resolve better the structure of the emission low temperature measurements have been performed. However, the total intensity of the spectra obtained are not higher than those obtained at RT due to the reduction of overlap between the excitation light and the optical absorption spectra.

At 5 K the Er^{3+} emission spectrum in KTP agrees well with the presence of eight overlapped bands, as expected from the emission of a single Er^{3+} centre. However, the emission spectrum in RTP shows larger number of resolved bands. Twelve components can be identified in figure 5(a). This situation most likely corresponds to the simultaneous contribution of the two erbium centres to the emission band, even though not all the expected bands appear well resolved.

The peak positions of figure 5(b) have been included in table 4. This can be identified as the energy difference of the sublevels of the $^4I_{15/2}$ multiplet corresponding to the erbium centres in KTP.

4. Conclusions

The spectroscopic properties of Er^{3+} in RTP and KTP single crystal hosts are similar. Two erbium centres (likely Er in the two titanium sites with inequivalent concentration) mainly contribute to the spectra. The strongest optical absorption is found for light polarized parallel to the crystallographic *c*-axis; this must be taken into account in the design of optical pumping systems. The radiative lifetimes calculated for Er^{3+} in RTP are similar to those calculated in other solid lattices.

Acknowledgment

This work has been supported by CICyT under project number TIC96-1039. The cooperation of Dr A Kling and Dr M J Martín in the acquisition and analysis of RBS measurements is gratefully acknowledged.

References

[1] Brown A J W, Bowers M S, Kangas K W and Fisher C H 1992 *Opt. Lett.* **17** 109
[2] Zhang L, Chandler P J, Townsend P D, Alwahabi Z T, Pityana S L and McCaffery A J 1993 *J. Appl. Phys.* **73** 2695
[3] Yang S T, Eckardt R C and Byer R L 1994 *Opt. Lett.* **19** 475
[4] Yamamoto Y, Yamaguchi S, Suzuki K and Yamada N 1994 *Appl. Phys. Lett.* **65** 938
[5] Takeuchi S and Kobayahi T 1994 *J. Appl. Phys.* **75** 2757
[6] Zaldo C, Aguiló M, Díaz F and Loro H 1996 *J. Phys.: Condens. Matter* **8** 10 693
[7] Zaldo C, Martín M J, Solé R, Aguiló M, Díaz F, Roura P, López de Miguel M 1998 *Opt. Mater.* **10** 29
[8] Zaldo C, Rico M, Martín M J, Massons J, Aguiló M and Díaz F 1998 *J. Lumin.* **79** 127
[9] Jacco J C, Loiacono G M, Laso M, Mizell G and Greenberg B 1984 *J. Cryst. Growth* **70** 484
[10] Hagerman M E, Kozhevnikov V L and Poeppelmeir K R 1993 *Chem. Mater.* **5** 1211
[11] Solé R, Nikolov V, Koseva I, Peshev P, Ruiz X, Zaldo C, Martín M J, Aguiló M and Díaz F 1997 *Chem. Mater.* **9** 2745
[12] Wang K, Wang W, Ding P, Landford W A and Liu Y 1995 *J. Appl. Phys.* **77** 3581
[13] Martín M J, Zaldo C, da Silva M F, Soares J C, Díaz F and Aguiló M 1997 *J. Phys.: Condens. Matter* **9** L465
[14] Tordjman I, Masse R and Guitel J C 1974 *Z. Kristallogr.* **139** S103
[15] Judd B R 1962 *Phys. Rev.* **127** 750
[16] Ofelt G S 1962 *J. Chem. Phys.* **37** 511
[17] Desurvire E 1994 *Phys. Today* **47** 20
[18] Martín M J, Zaldo C, Díaz F, Solé R, Bravo D and López F J 1995 *Radiat. Eff. Defects Solids* **136** 243
[19] Kaminskii A A 1996 *Crystalline Lasers: Physical Processes and Operating Schemes* (Boca Raton, FL: Chemical Rubber Company)
[20] Cheng L K, Cheng L T, Galperin J, Morris P A and Beirlein J D 1994 *J. Cryst. Growth* **137** 107
[21] Weber M J 1967 *Phys. Rev.* B **157** 262
[22] Carnall W T, Fields P R and Rajnak K 1968 *J. Chem. Phys.* **49** 4424
[23] Devi A R and Jayasankar C K 1996 *J. Non Cryst. Solids* **197** 111
[24] Carnall W T, Fields P R and Wybourne B G 1965 *J. Chem. Phys.* **42** 3797